Supporting Information

An all-organic symmetric battery base on a triquinoxalinylene derivative with different redox voltage active sites and large conjugation system

Yi Zhang[a], Zhaopeng Sun[a], Xiangyue Kong[a], Yilin Lin[a] and Weiwei Huang[a,b*]

[a] *School of Environmental and Chemical Engineering, Yanshan University, Qinhuangdao 066004, China*

[b] *Key Laboratory of Advanced Energy Materials Chemistry (Ministry of Education), College of Chemistry, Nankai University, Tianjin, 300071, China*

**Corresponding author.*

E-mail address: huangweiwei@ysu.edu.cn (W. Huang)

Contents

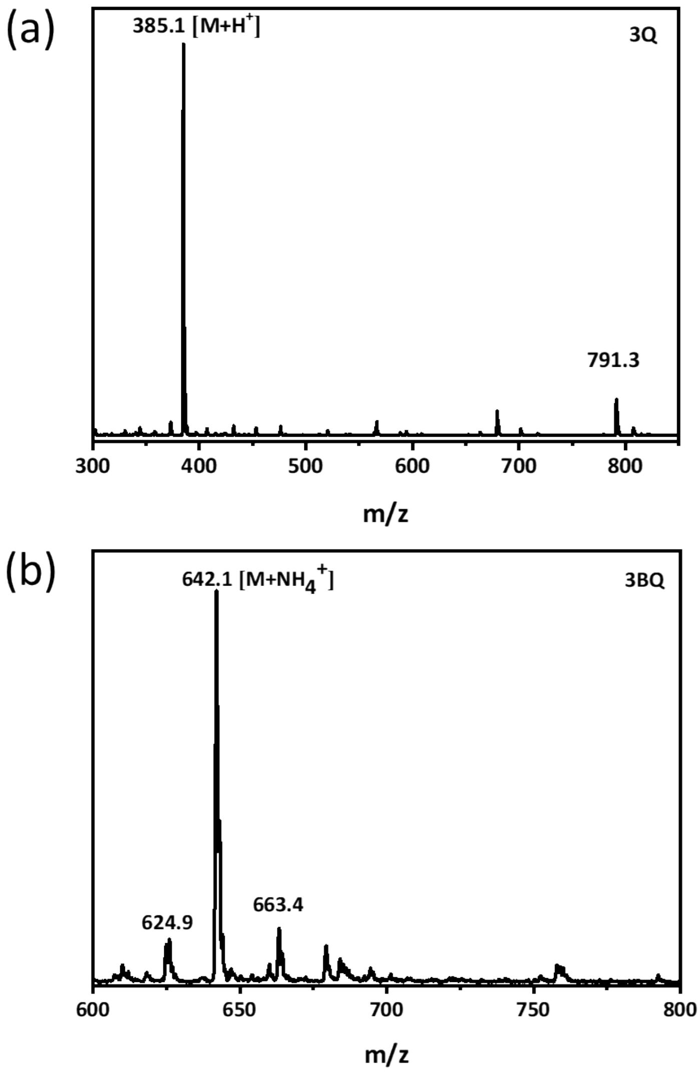

Fig. S1. The ESI-MS spectra of (a) **3Q** and (b) **3BQ**.

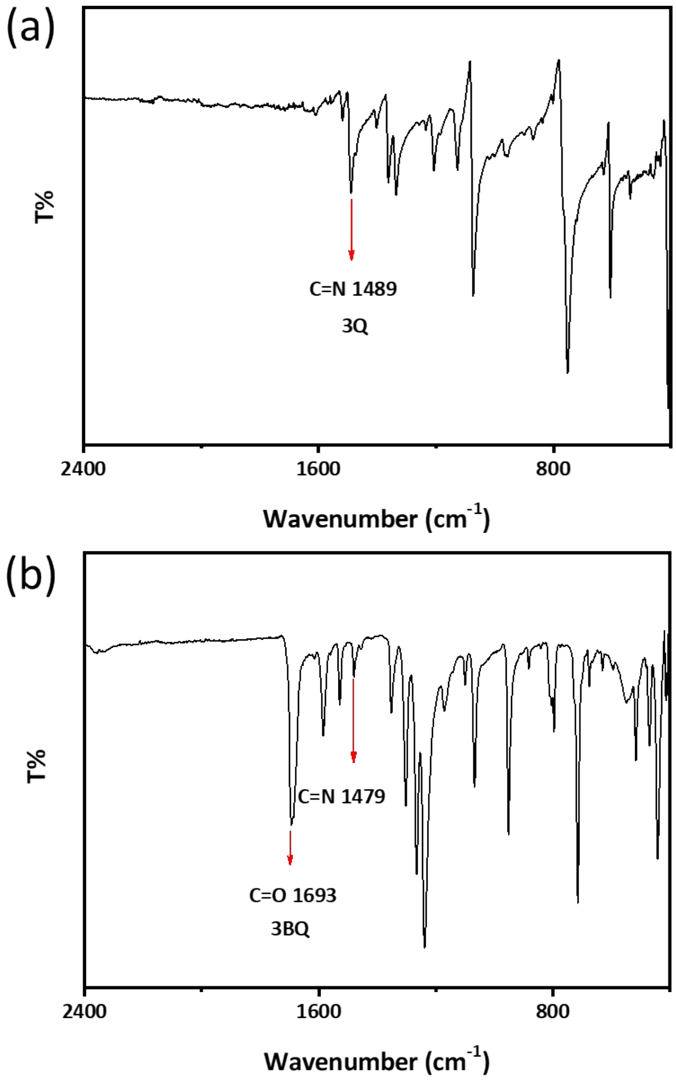

Fig. S2. The FTIR spectrums of (a) **3Q** and (b) **3BQ**.

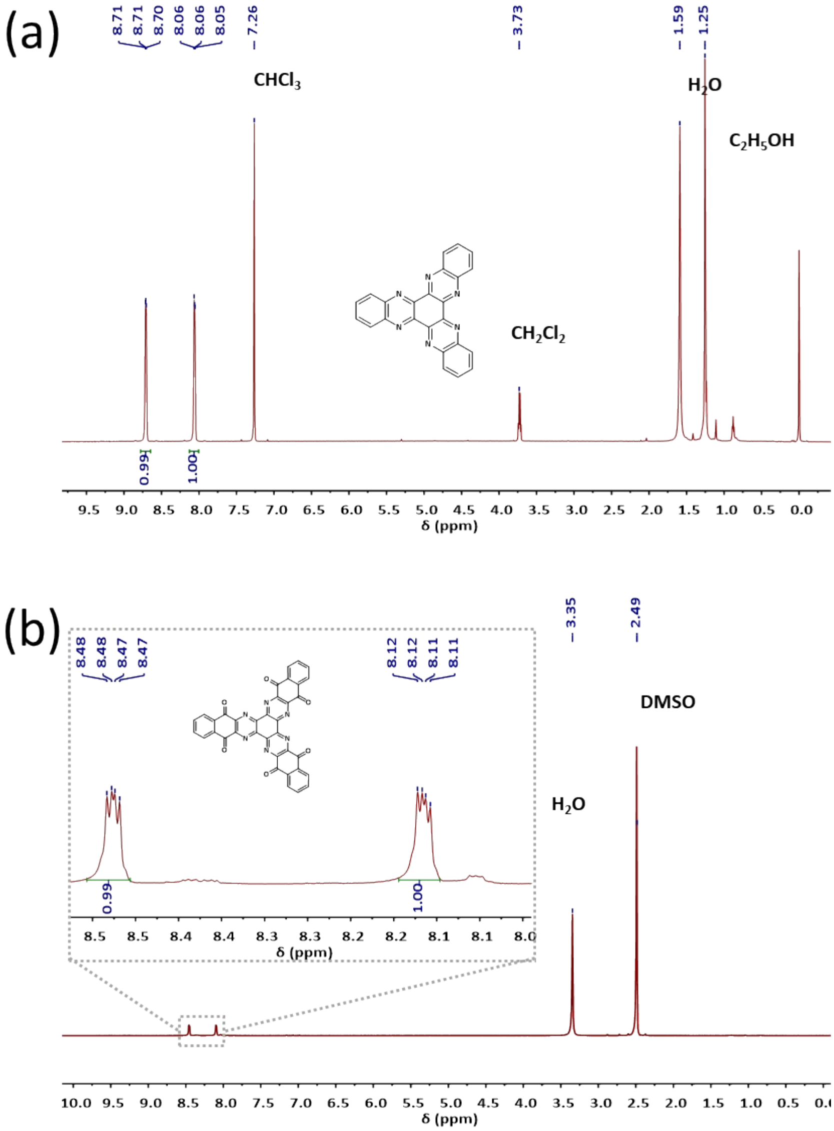

Fig. S3. The [1]H NMR spectrums of (a) **3Q** ($CDCl_3$) and (b) **3BQ** (DMSO-d_6).

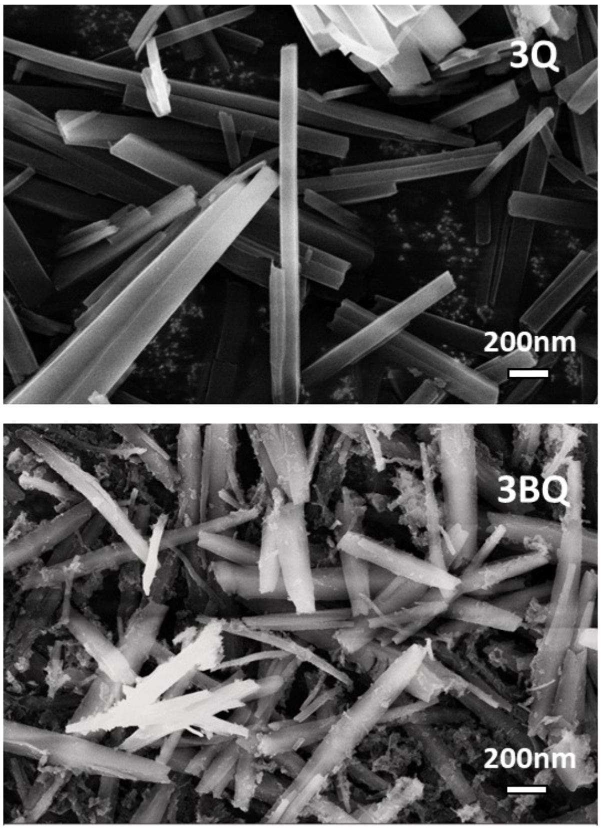

Fig. S4. SEM images of **3Q** and **3BQ.**

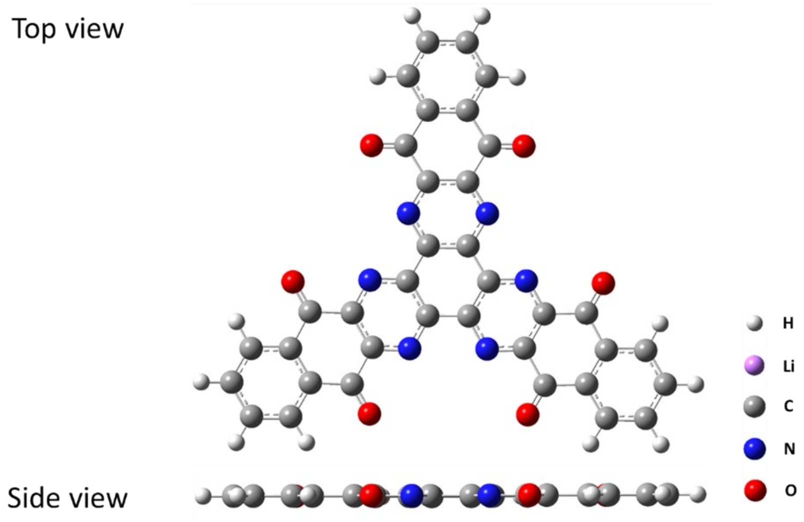

Fig. S5. Schematic of the optimized structure of **3BQ**.

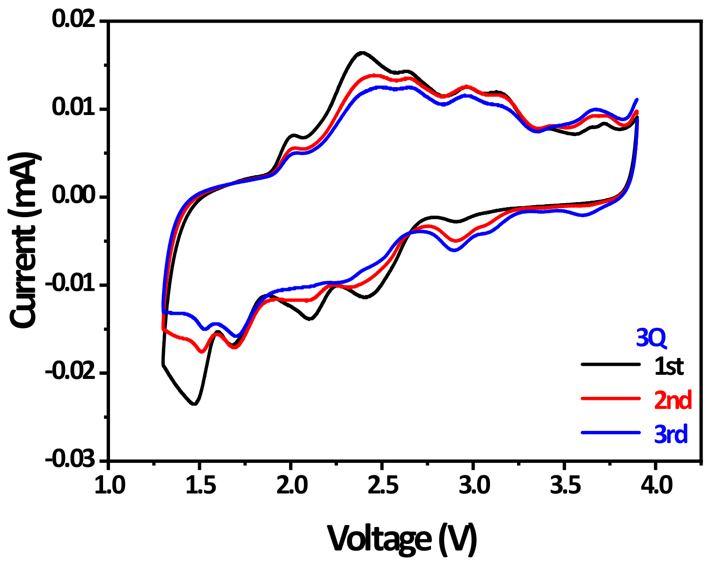

Fig. S6. CV curve of **3Q** at a scan rate of 0.2 mV s^{-1}.

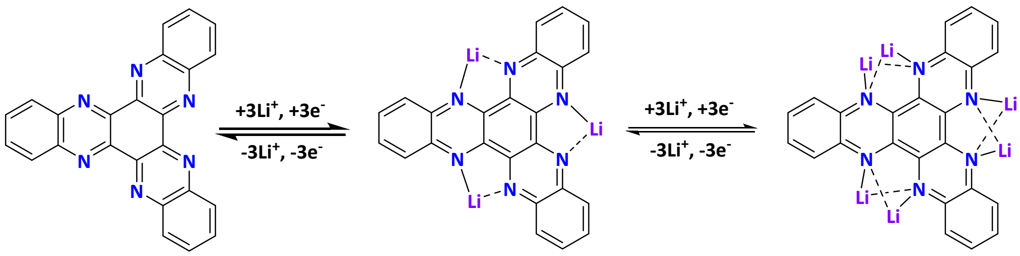

Fig. S7. The electrochemical redox mechanism of **3Q**.[1]

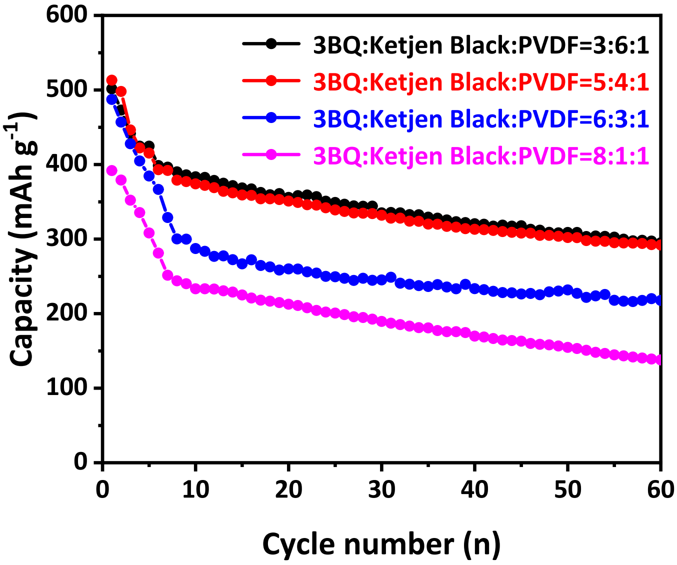

Fig. S8. Cycle performance of **3BQ** with different Ketjen Black content at 0.2 C.

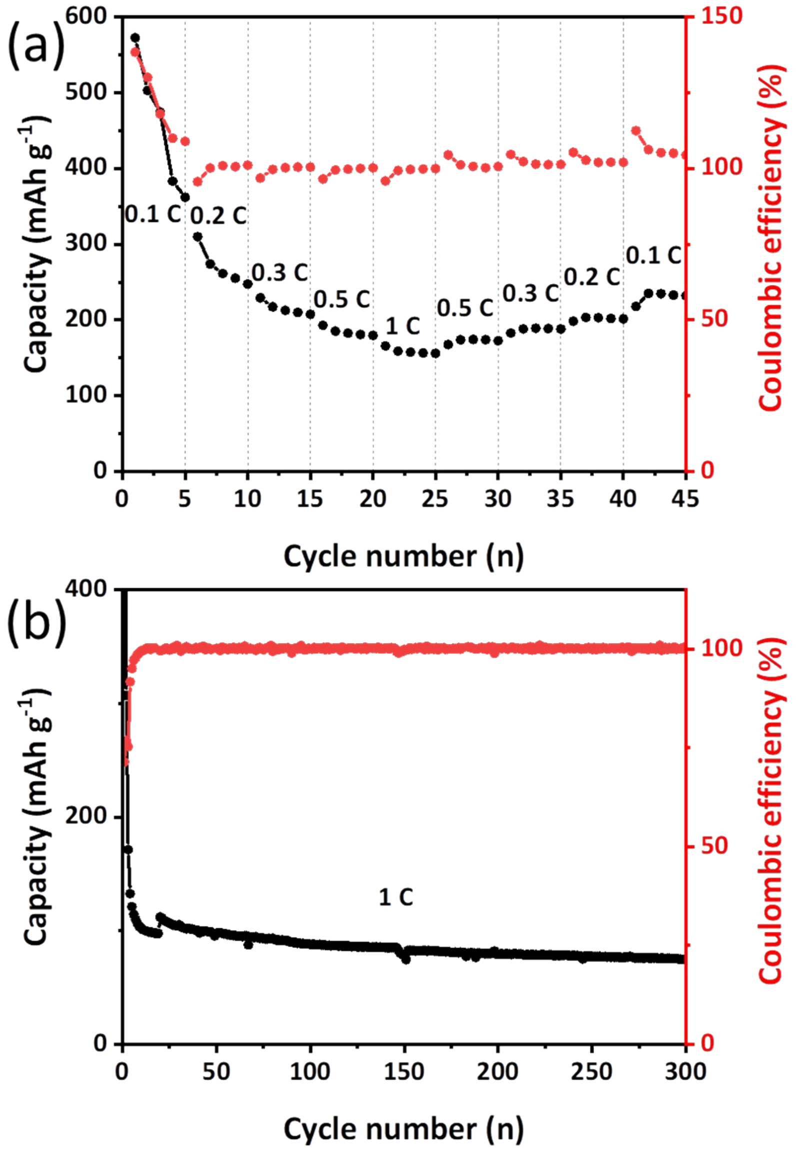

Fig. S9. Electrochemical performance of **3BQ** cathode in Li-ion half-cell between 1.3 and 3.9 V (vs Li/Li^+) in 1 M LiTFSI in DOL/DME (1:1, v/v). (a) Rate performance at different current densities; (b) cycling performance at 1 C.

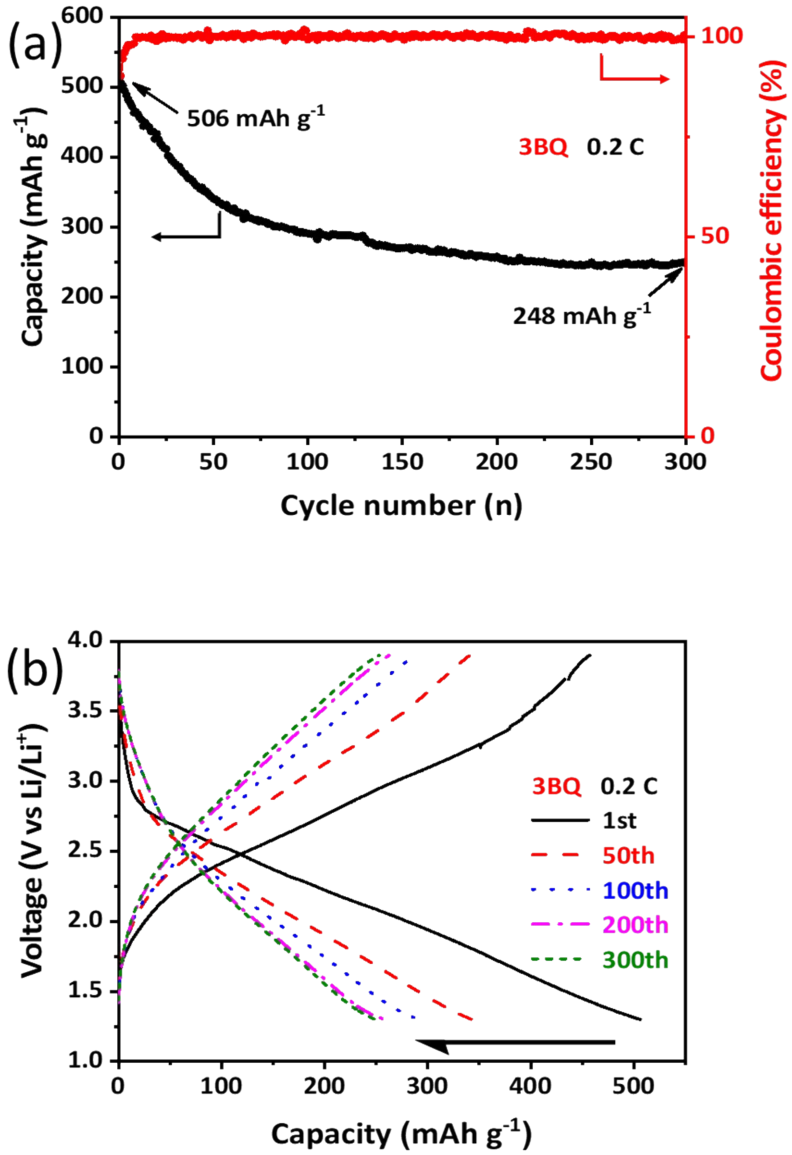

Fig. S10. (a) Cycle performance and (b) charge-discharge curves of **3BQ** cathode at 0.2 C.

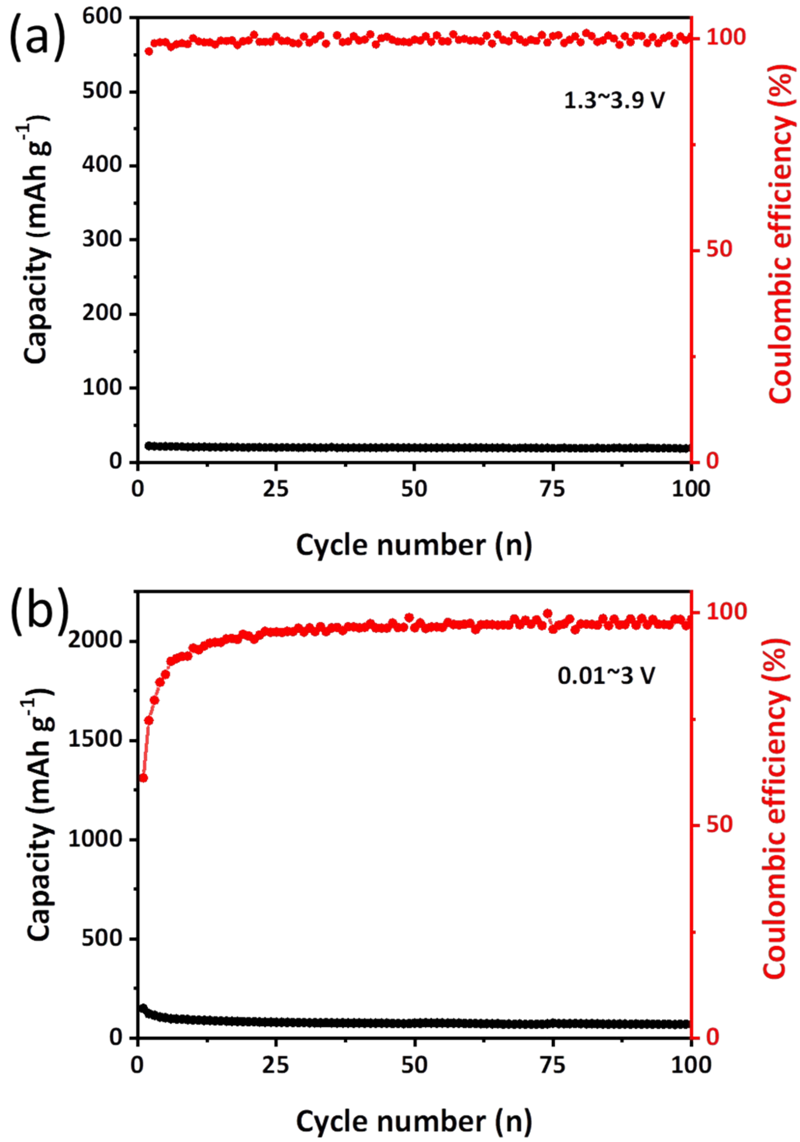

Fig. S11. Cyclic performance of Ketjen Black in different voltage ranges (Ketjen Black : PVDF = 9:1).

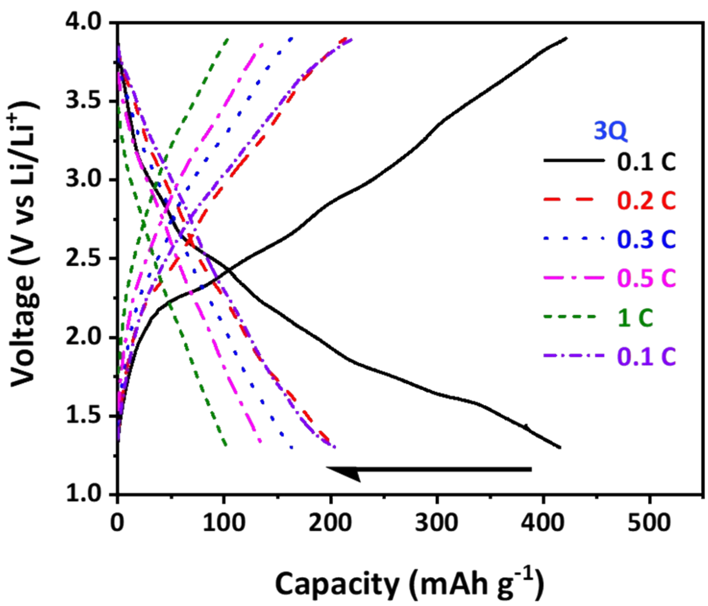

Fig. S12. Charge-discharge curves of **3Q** at different rates.

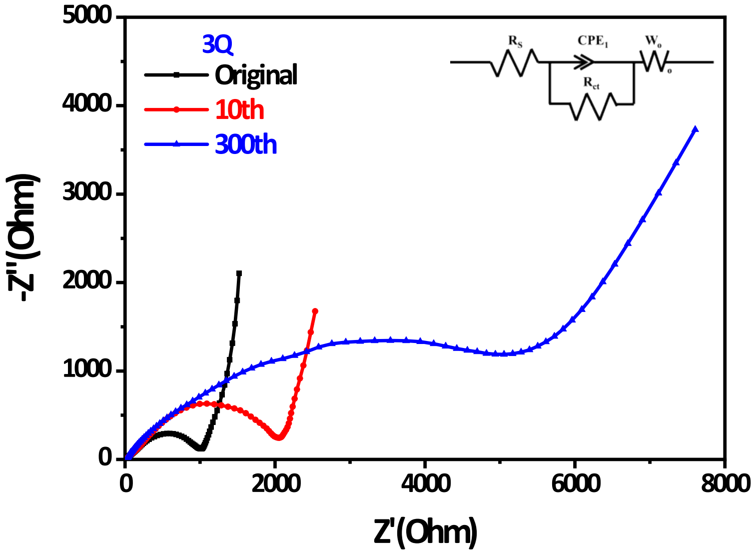

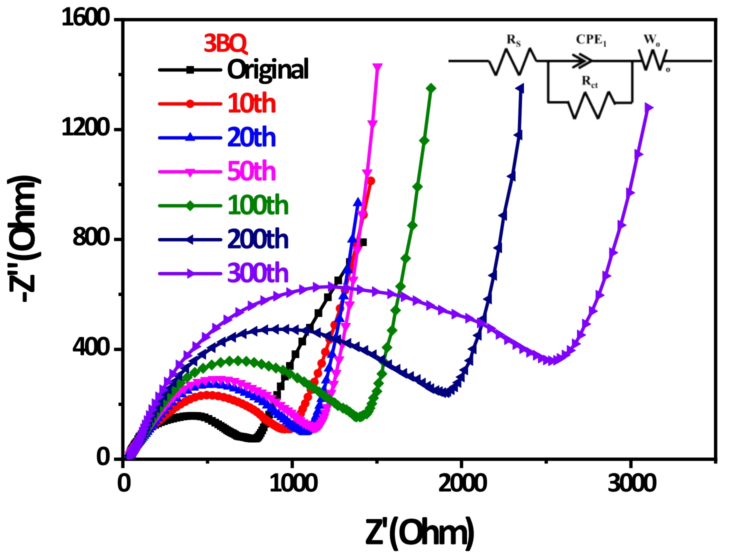

Fig. S13. The Nyquist plots of **3Q** and **3BQ** as cathodes during the cycles. Insets are the corresponding equivalent circuit, R_{ct} is the charge-transfer resistance, W_0 is the Warburg impendence and CPE_1 is the double-layer capacitance.

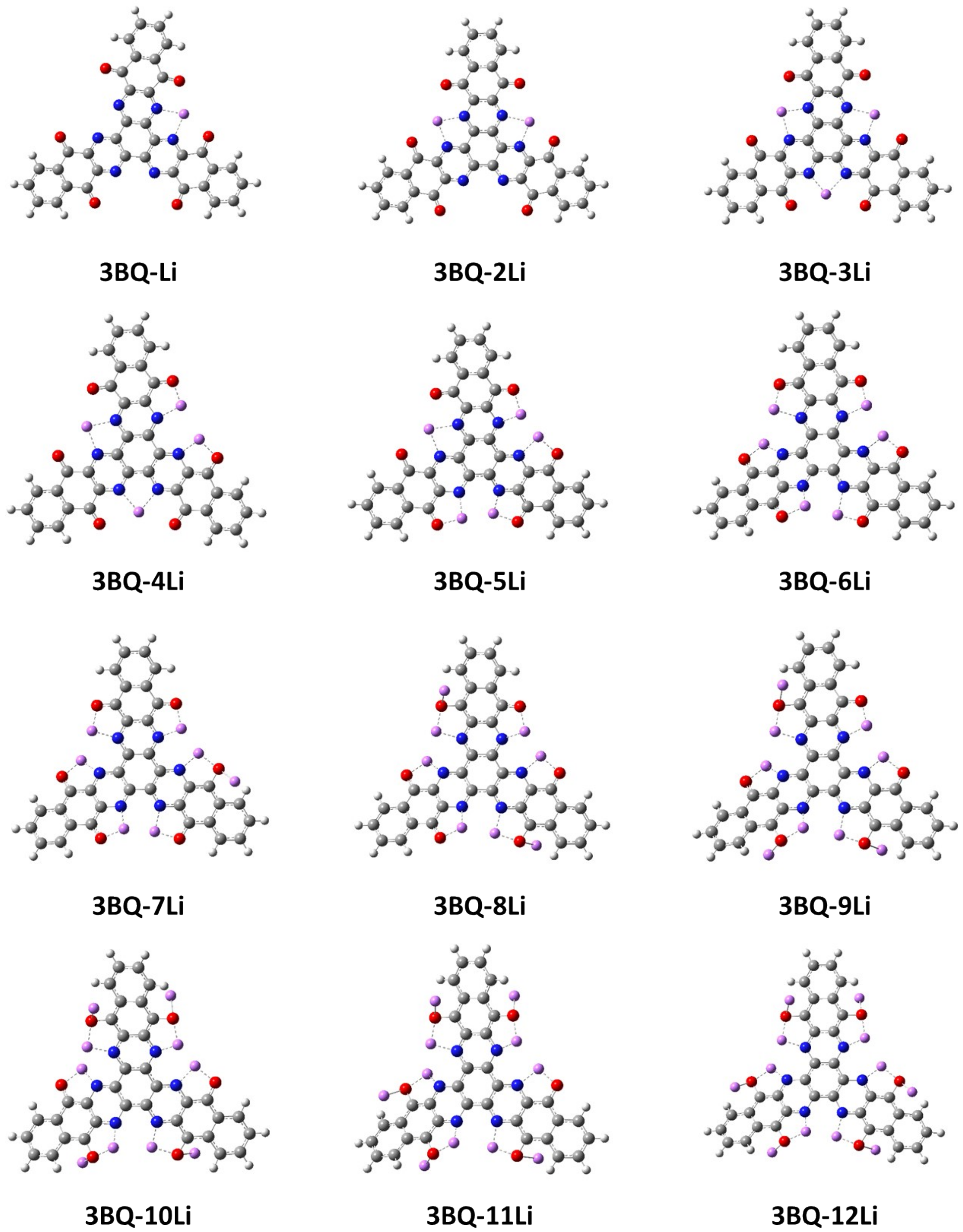

Fig. S14. The optimized structure of 3BQ-xLi (x=1~12) based on DFT calculation at the B3LYP/6-311G (d, p).

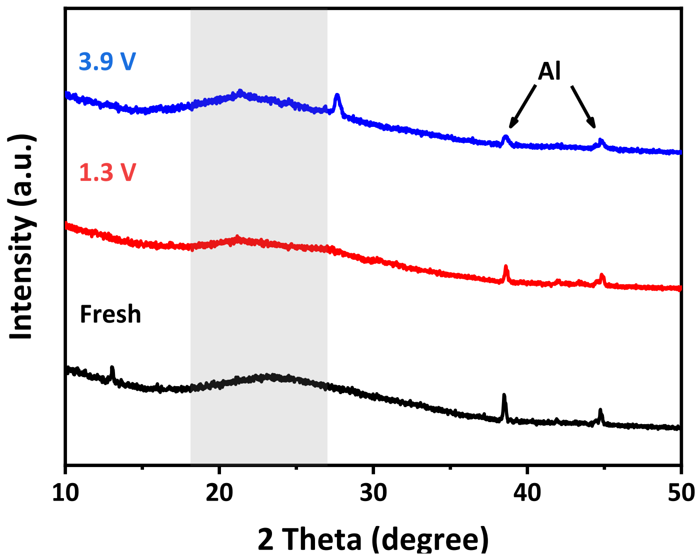

Fig. S15. Ex-situ XRD patterns of **3BQ** cathode at different states.

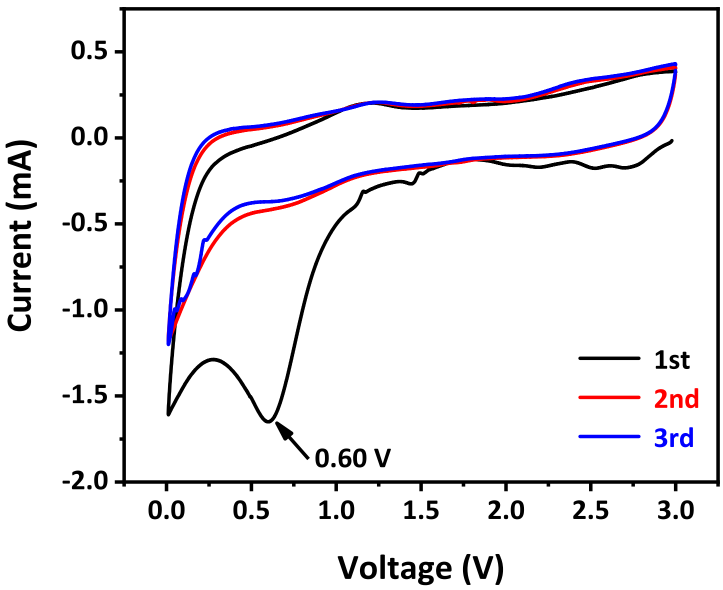

Fig. S16. The CV curves of **3BQ** anode in the voltage range of 0.01~3 V at a scan rate of 0.2 mV s^{-1}.

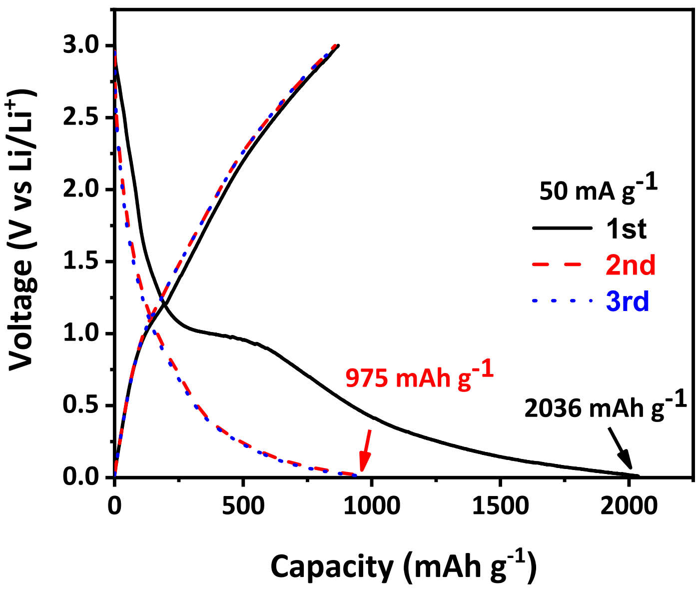

Fig. S17. The charge-discharge curves of **3BQ** anode in the initial 3 cycles at a current density of 50 mA g^{-1}.

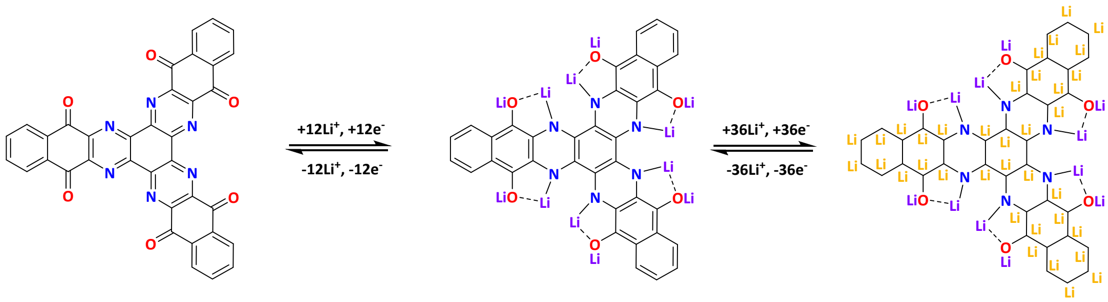

Fig. S18. Proposed superlithiation reaction mechanism of **3BQ** anode.

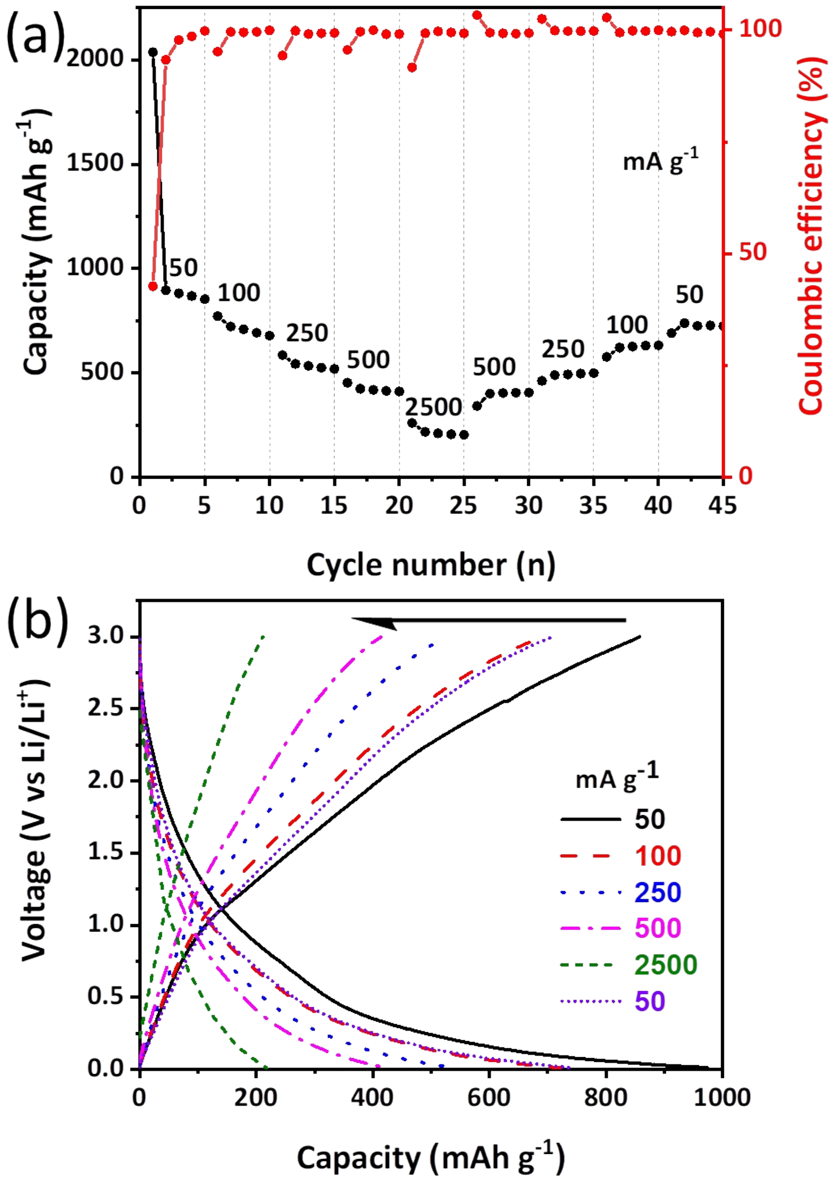

Fig. S19. (a) Rate performance and (b) charge-discharge curves of **3BQ** anode at different current densities.

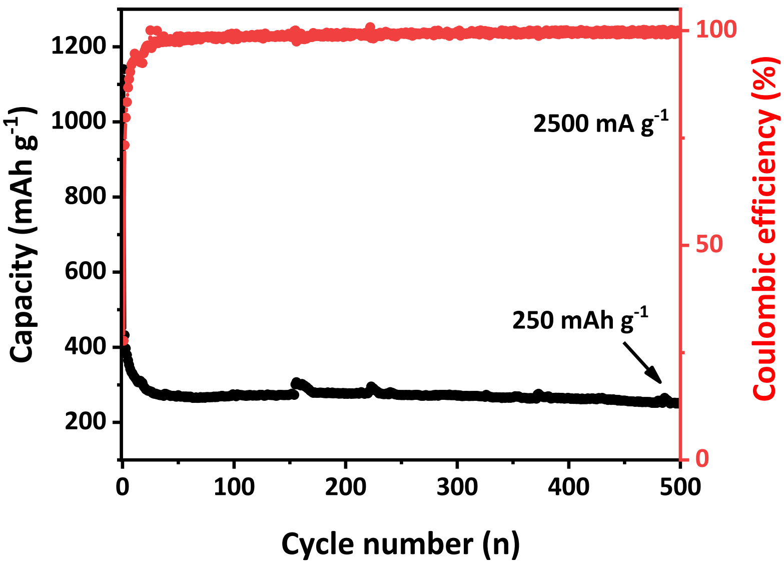

Fig. S20. Cycle performance of **3BQ** anode at 2500 mA g^{-1} for 500 cycles.

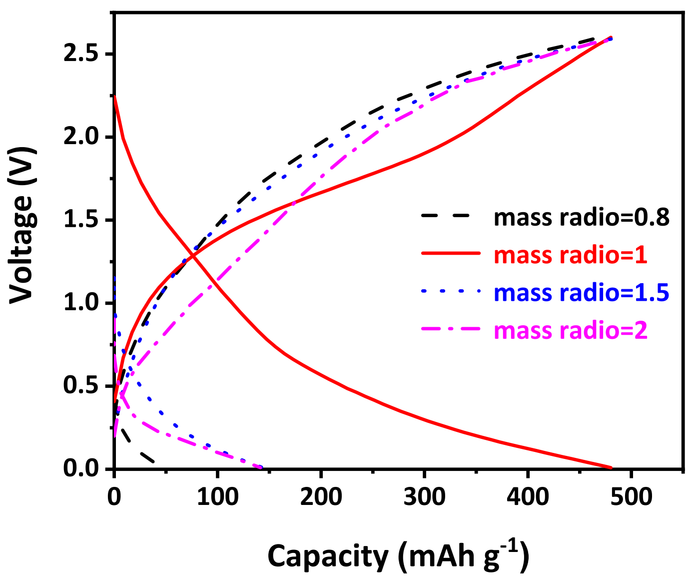

Fig. S21. Charge-discharge curves at different mass ratios of anode and cathode at 0.2 C.

Table S1. Comparison of electrochemical performance of other organic cathodes.

Molecular structure	Cathode composition	Mass ratio	Electrolytes	Initial capacity ($mAh\ g^{-1}$) /Current density	Capacity ($mAh\ g^{-1}$)/Cycle number/ Current density	Ref.
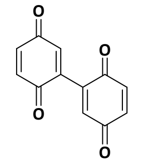	BBQ:graphene:PVDF	60:30:10	1 M LiTFSI in DOL/DME	293/0.1	149/100/0.1	[2]
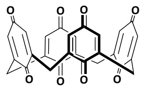	C4Q:SuperP:PVDF	60:25:15	1 M $LiPF_6$ in EC/DMC	427/0.1	28/50/0.1	[3]
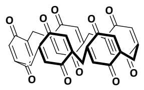	P5Q:Carbon Black:PVDF	30:60:10	4.2 M LiTFSA in AN	405/0.2	310/900/0.2	[4]
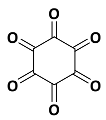	C_6O_6:KB:PVDF	50:40:10	0.3 M LiTFSI in [PY13] [TFSI]	902/0.02	239/200/0.5	[5]
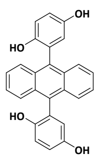	ABBOH:CMK-3/SP/La133	4:4:1:1	3 M LiTFSI in DOL/DME	--	194/250/0.2	[6]
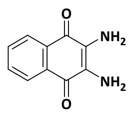	DANQ:SP:PVDF	60:30:10	1 M LiTFSI in DME/DIOX	250/0.2	248/500/0.2	[7]
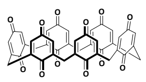	C6Q:KB:PVDF	60:30:10	1 M $LiPF_6$ in EC/DMC	423/0.1	216/100/0.1 195/300/0.1	[8]
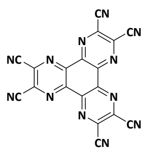	6CN:KB:PTFE	48.1:47.9:3.5	PEO membranes	300/0.2	250/30/0.2	[9]
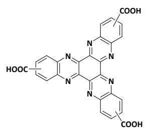	HATNTA:GO:PVDF	50:40:10	1 M $LiPF_6$ in EC/DEC.	226/0.16	193/90/0.2	[10]
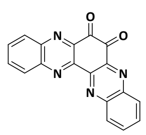	2Q:RGO:PVDF	30:60:10	1 M LiTFSI in DOL/DME	372/1	359/200/1	[1]

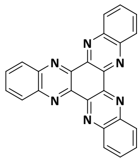	3Q:RGO:PVDF	30:60:10	1 M LiTFSI in DOL/DME	395/1	222/10000/20	[1]
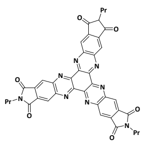	HATNTI-Pr:KB:PVDF	60:30:10	1 M LiTFSI in DOL/TEGDME	317/0.1	254/0.1/100	[11]
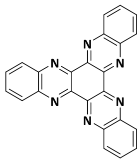	HATN:GO:PVDF	50:40:10	1 M $LiPF_6$ in EC/DEC.	410/0.1	226/90/0.1	[10]
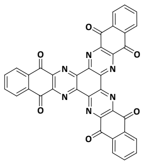	3BQ:KB:PVDF	50:40:10	1 M $LiPF_6$ in EC/DMC	506/0.2	248/300/0.2	This work
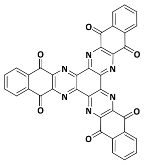	HATAQ:KB:PVDF	30:60:10	1 M LiTFSI in DOL/DME(1/2 V/V) with 0.3 wt% $LiNO_3$	426/0.4	209/1000/19	[12]

Table S2. The total energies and the binding energies (ΔE) in Hartree (eV) calculated at the B3LYP/6-311G (d, p) level in EC/DMC solvent.

Spin state	Energy ($eV\times10^4$)	Reaction processes	$\Delta E = E_{xLi} - (E_{(x-1)Li} + E_{Li(0)})$
3BQ	-2159.2299 (-5.8756)		
3BQ-1Li	-2166.8894 (-5.8965)	3BQ→3BQ-1Li	-0.1497 (-4.0217)
3BQ-2Li	-2174.5395 (-5.9173)	3BQ-1Li→3BQ-2Li	-0.1403 (-3.8173)
3BQ-3Li	-2182.2044 (-5.9382)	3BQ-2Li→3BQ-3Li	-0.1551 (-4.2206)
3BQ-4Li	-2189.8247 (-5.9589)	3BQ-3Li→3BQ-4Li	-0.1103 (-3.0011)
3BQ-5Li	-2197.4541 (-5.9797)	3BQ-4Li→3BQ-5Li	-0.1105 (-3.0076)
3BQ-6Li	-2205.0745 (-6.0004)	3BQ-5Li→3BQ-6Li	-0.0908 (-2.4709)
3BQ-7Li	-2212.6751 (-6.0211)	3BQ-6Li→3BQ-7Li	-0.0829 (-2.2545)
3BQ-8Li	-2220.2678 (-6.0417)	3BQ-7Li→3BQ-8Li	-0.0829 (-2.2559)
3BQ-9Li	-2227.1716 (-6.0606)	3BQ-8Li→3BQ-9Li	-0.0606 (-1.6490)
3BQ-10Li	-2235.4240 (-6.0830)	3BQ-9Li→3BQ-10Li	-0.0743 (-2.0219)
3BQ-11Li	-2242.9947 (-6.1036)	3BQ-10Li→3BQ-11Li	-0.0609 (-1.6572)
3BQ-12Li	-2250.5603 (-6.1242)	3BQ-11Li→3BQ-12Li	-0.0558 (-1.5184)

$E_{Li(0)}$= -7.5098 Hartree

Table S3. Sum of electronic and thermal Gibb free energies in Hartree (eV) of optimized structures and the redox potentials (V) calculated at the B3LYP/6-311G (d, p) level in EC/DMC solvent.

Spin state	Energy (eV×10^4)	Reaction processes	Calculated potential (V vs. Li/Li^+)
3BQ	-2159.2944 (-5.8759)		
3BQ-1Li	-2166.9558 (-5.8967)	3BQ→3BQ-1Li	3.7589
3BQ-2Li	-2174.6061 (-5.9175)	3BQ-1Li→3BQ-2Li	3.4584
3BQ-3Li	-2182.2733 (-5.9384)	3BQ-2Li→3BQ-3Li	3.9172
3BQ-4Li	-2189.8926 (-5.9591)	3BQ-3Li→3BQ-4Li	2.6121
3BQ-5Li	-2197.5188 (-5.9799)	3BQ-4Li→3BQ-5Li	2.8035
3BQ-6Li	-2205.1397 (-6.0006)	3BQ-5Li→3BQ-6Li	2.6576
3BQ-7Li	-2212.7440 (-6.0213)	3BQ-6Li→3BQ-7Li	2.2038
3BQ-8Li	-2220.3379 (-6.0420)	3BQ-7Li→3BQ-8Li	1.9232
3BQ-9Li	-2227.9281 (-6.0626)	3BQ-8Li→3BQ-9Li	1.8236
3BQ-10Li	-2235.4936 (-6.0832)	3BQ-9Li→3BQ-10Li	1.1502
3BQ-11Li	-2243.0638 (-6.1038)	3BQ-10Li→3BQ-11Li	1.2780
3BQ-12Li	-2250.6307 (-6.1244)	3BQ-11Li→3BQ-12Li	1.1882

$E_{Li(0)}$= -7.5232 Hartree

Table S4. Comparison of electrochemical performance of other all-organic batteries.

Molecular structure	Cathode composition	Mass ratio	Electrolytes	Initial capacity (mAh g^{-1}) /Current density	Capacity (mAh g^{-1})/Cycle number/ Current density	Ref.
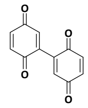	BBQ:CMK-3:GO:La133	40:50:10:10	1 M LiTFSI in DOL/DME	316/1	~80/1000/2	[13]
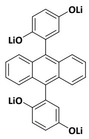	ABB_4OLi:CMK-3:SP:La133	40:40:10:10	3 M LiTFSI in DOL/DME	282/0.2	63/200/0.2	[6]
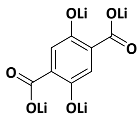	$Li_4C_8H_2O_6$:CB:PVDF	65:30:5	1 M $LiPF_6$ in EC/DMC	223/0.1	212/50/0.1	[14]
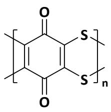	PDB:CNTs:PVDF	30:50:20	1 M LiTFSI in DOL/DME	249/0.06	119/250/3	[15]
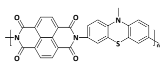	PI1:KB:PVDF	40:40:20	1 M $LiPF_6$ in EC/DMC	77/0.2	72/1000/0.2	[16]
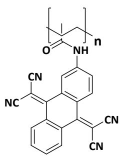	TCAQ:SP:PVDF	40:55:5	1 m $LiClO_4$ in EC/DMC (3/7 v/v)	105/1	71/250/1	[17]
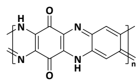	Poly-BQ1:SP:PVDF	50:40:10	1 M LiTFSI in DOL/DME	351.5/0.1	203.4/400/2	[18]
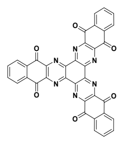	3BQ:KB:PVDF	50:40:10	1 M $LiPF_6$ in EC/DMC	483/0.2	172/300/0.2	This work

Equation S1. Lithium ion diffusion coefficient for **3Q** and **3BQ**.

$$D = \frac{R^2T^2}{2A^2n^4F^4C^2\sigma^2}$$

where A is the surface area of the electrode, n is the number of the electrons per molecule attending the electronic transfer reaction, F is the Faraday constant, C is the concentration of lithium ion in electrode, R is the gas constant, T is the room temperature in our experiment, σ is the slope of the line $Z' \sim \omega^{-1/2}$ which can be obtained from the line of $Z' \sim \omega^{-1/2}$, respectively.

References

1 C. Peng, G. Ning, J. Su, G. Zhong, W. Tang, B. Tian, C. Su, D. Yu, L. Zu, J. Yang, M. Ng, Y. Hu, Y. Yang, M. Armand and K. Loh, *Nat. Energy*, 2017, **2**, 17074.
2 J. Yang, P. Xiong, Y. Shi, P. Sun, Z. Wang, Z. Chen and Y. Xu, *Adv. Funct. Mater.*, 2020, **30**, 1909597.
3 S. Zheng, J. Hu and W. Huang, *Inorg. Chem. Front.*, 2017, **4**, 1806.
4 W. Zhang, H. Sun, P. Hu and W. Huang, *EcoMat*, 2021, 1.
5 Y. Lu, X. Hou, L. Miao, L. Li, R. Shi, L. Li, and J. Chen, *Angew. Chem. Int. Ed.*, 2019, **58**, 7020.
6 Y. Hu, W. Tang, Q. Yu, C. Yang and C. Fan, *ACS Appl. Mater. Inter.*, 2019, **58**, 32987.
7 J. Lee, H. Kim and M. Park, *Chem. Mater.*, 2016, **28**, 2408.
8 X. Zhang, W. Zhou, M. Zhang, Z. Yang and W. Huang, *J. Energy Chem.,* 2021, **52**, 28.
9 Y. Hanyu, T. Sugimoto, Y. Ganbe, A. Masuda and I. Honma, *J. Electrochem. Soc*., 2013, **161**, A6.
10 J. Wang, K. Tee, Y. Lee, S.N. Riduan and Y. Zhang, *J. Mater. Chem. A*, 2018, **6**, 2752.
11 Z. Wang, Q. Qi, W. Jin, X. Zhao, X. Huang and Y. Li, *ChemSusChem*, 2021, **14**, 3858.
12 M. Wu, N. Lu, T. Chen, H. Lyu, T. Huang, S. Dai, X. Sun, A. Ivanov, J. Lee, I. Popovs and W. Kaveevivitchai, *Adv. Energy. Mater.*, 2021, **11**, 2100330.
13 Z. Yao, W. Tang, X. Wang, C. Wang, C. Yang and C. Fan, *J. Power Sources*, 2020, **448**, 227456.
14 S. Wang, L. Wang, K. Zhang, Z. Zhu, Z. Tao and J. Chen, *Nano Lett.*, 2013, **13**, 4404.
15 J. Xie, Z. Wang, Z. Xu and Q. Zhang, *Adv. Energy. Mater.*, 2018, **8**, 1703509.
16 N. Casado, D. Mantione, D. Shanmukaraj and D. Mecerreyes, *ChemSusChem*, 2020, **13**, 2464.
17 A. Wild, M. Strumpf, B. Häupler, M. Hager and U. Schubert, *Adv. Energy. Mater.*, 2017, **7**, 1601415.
18 Y. Zhao, M. Wu, H. Chen, J. Zhu, J. Liu, Z. Ye, Y. Zhang, H. Zhang, Y. Ma, C. Li and Y. Chen, *Nano Energy*, 2021, **86**, 106055.